2020-03-28

Passive Vortex-Induced Vibration Control

Lucas A. Lorditch
Worcester Polytechnic Institute

Passive Vortex-Induced Vibration Control for Maximizing Lock-In Range in Transient Flow Velocities

Lucas Lorditch

Abstract

Historical experiments on vortex-induced vibrations (VIV) have studied the effects that the angle of incidence of a cylinder in fluid flow has on the shedding frequency, expressed through the dimensionless parameter Strouhal number. This report analyses these past experiments. A prototype design is submitted for a passively adjusting system that responds to changes in flow velocity. Two sets of real system characteristics used in practical experiments are examined to see the effect that scaling would have on the range of flow velocities that can be compensated for by the prototype. The purpose of this would be to increase the range of flow velocities in which the maximum amount of energy is transferred into vibrational energy; this vibrational energy can then be harvested, yielding greater amounts of usable energy than a static device. It was found through modeling that scaling would have a substantial effect on the range of flow velocities where lock-in occurs. The larger scale model predicts a system could be capable of dynamically adjusting for a change in 0.311 m/s over a range of 20 degrees through the use of a 1 N*m/radian spring. These results are theoretical and it is recommended that a practical experiment be conducted to verify them.

Table of Contents

Table of Figures

Intro

Historically, study of VIV (Vortex-Induced Vibration) has been a primary concern of aeronautical and civil engineers concerned with reducing amplitude and avoiding resonance of vibrations in a fluid stream (Harish, 2020) (Jing, et al., 2017). Recently, potential for VIV as an alternate energy source has been explored (Bernitsas, Raghavan, Ben-Simon, & Garcia, 2008). Several MQP's at WPI have approached this topic with varying results (Hall-Stinson, Lehrman, & Tripp, 2011) (Mayforth, Doty, & Pratt, 2011) (O'Connor, Wedell, Gagnon, & Diltz, 2017) (Pierce, Neeld, Shipulski, & Ciliberto, 2019) (Warner, Ball, Sakhuja, & Killen, 2012). Variables controlling VIV are analyzed and design considerations are proposed for a system which will passively respond to changes in flow velocity, extending the range in which lock-in occurs. The main property which is examined is the angle of incidence and its effect on various functions of VIV, primarily the Strouhal number. The goal is modeling and expressing a method which will dynamically and passively alter the angle of incidence of the structure in response to fluctuations in flow velocity.

Background

Theory

As fluid flows over a structure, its boundary layers can separate from the rest of the flow, causing a differential in pressures which results in the formation of a vortex. In certain conditions (Figure 1), this can occur in an oscillatory manner, creating what is known as a Karman vortex street. Usually seen as detrimental (Jing, et al., 2017), recent experiments have realized this phenomenon's potential as an alternative energy source (Bernitsas, Raghavan, Ben-Simon, & Garcia, 2008).

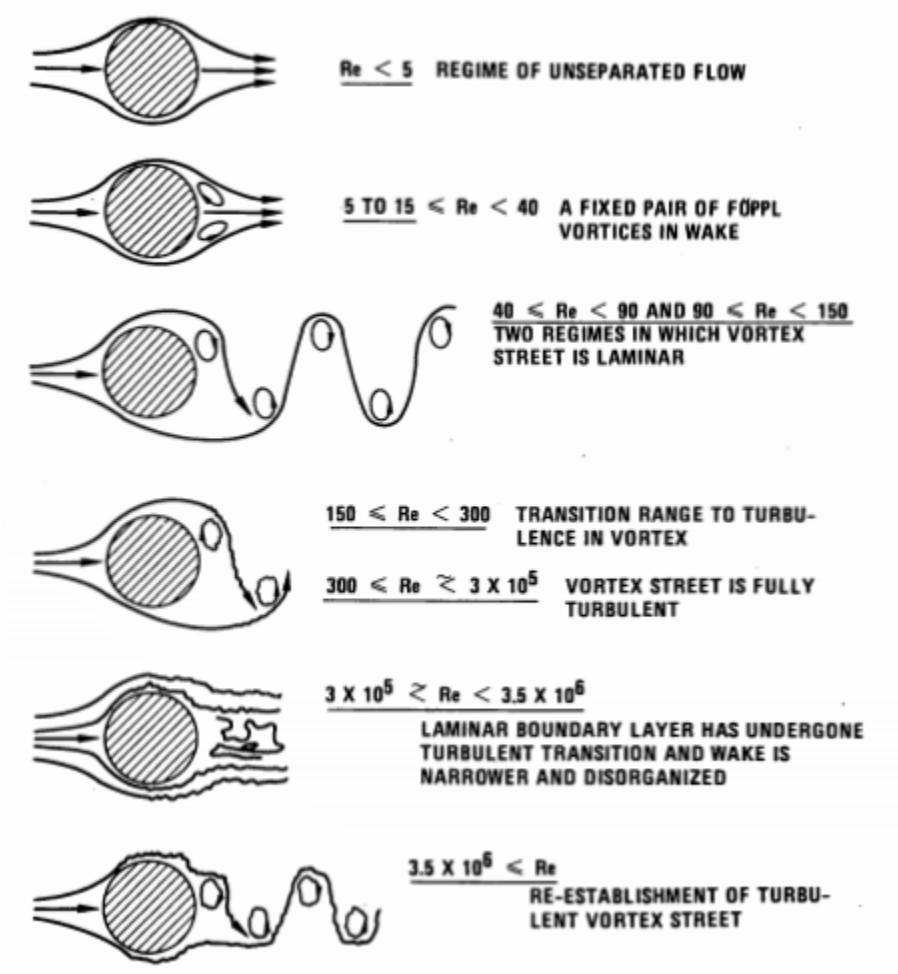

Figure 1: Regimes of fluid flow across smooth circular cylinders (Lienhard, 1966) in (Blevins, 2001)

The rate at which these vortices shed off the forming structure has a frequency and period, which can be seen in Figure 2. Direct parallels can be drawn between the frequency at which the vortices shed and natural frequency of the structure from which they are shedding. It is possible to control the properties of the shedding structure to drive the creation of these vortices given a fluid flow. Further design considerations can be used to control the natural frequency of the shedding structure.

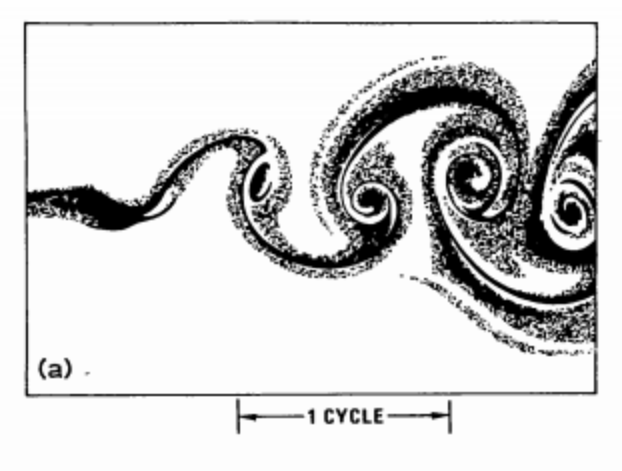

Figure 2: Stable staggered vortex street behind a cylinder vibrating transverse to the mean flow at resonance with vortex shedding, Re=190 (Griffin & Ramberg, 1974) in (Blevins, 2001)

A common (Bernitsas, Raghavan, Ben-Simon, & Garcia, 2008) (Hall-Stinson, Lehrman, & Tripp, 2011) (O'Connor, Wedell, Gagnon, & Diltz, 2017) (Pierce, Neeld, Shipulski, & Ciliberto, 2019) (Warner, Ball, Sakhuja, & Killen, 2012) design choice is a shedder geometry constrained to one dimension of freedom and held by coil springs. This allows tuning of the shedding structure's natural frequency by changing the spring's properties. Additional change can be made to the natural frequency by altering the mass of the shedder geometry.

If tuned properly, the shedding frequency and natural frequency of the shedder can be made to overlap, creating resonance. This maximizes the amplitude experienced by the shedder system. These conditions also create a phenomenon called "lock-in". Lock-in is a phenomenon which occurs when the transverse cylinder vibration is at or near the vortex shedding frequency, thereby affecting the vortex shedding frequency, causing it to shift to the frequency of cylinder vibration (Bishop & Hassan, 1964) in (Blevins, 2001). As the vortex shedding frequency approaches the natural frequency of a structure with elasticity, the vortex shedding frequency suddenly locks onto the structure frequency. It organizes the wake and generates a positive feedback loop which in turn can create large amplitude vibrations. These typically result at reduced velocity in the range $4 < U/(f_n D) < 8$ but have been seen to occur at sub and super harmonics of the shedding frequency (Blevins, 2001).

In this report, it will be shown that the frequency at which vortices are shed is a function of the Strouhal number. It will be further investigated how this Strouhal number can be manipulated through altering the angle of incidence at which the shedding structure interacts with fluid flow. A way to implement this with dynamic response to changing flow velocities is suggested.

Shedding frequency

The shedding frequency of vortices being formed by the shedder structure is a function of Strouhal number, free stream velocity in meters/sec and cylinder diameter in meters. It is expressed through the following equation:

$$f_s = \frac{SU}{D}$$

Equation 1: Shedding frequency (Blevins, 2001)

Where

$$S = Strouhal\ number$$

$$U = free\ stream\ velocity, meters/sec$$

$$D = cylinder\ diameter, meters$$

The shedding frequency can be expressed in the radians equivalent, or

$$\omega_s = 2\pi f_s$$

Lienahrd, as well as Achenbach and Heinecke found a relationship between Strouhal number and Reynolds number. As seen in Figure 3, the Strouhal number for a smooth or rough surface cylinder is constant in regime $500 < Re < 10^5$. At lower Reynolds numbers, the Strouhal number decreases by as much as 0.1 from 500 to 40. As Reynolds number increases above 10^5, Strouhal number increases as well.

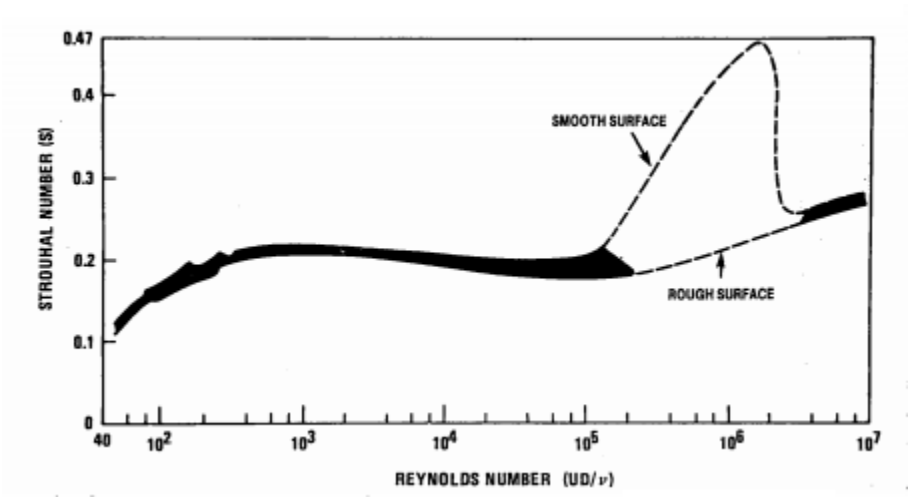

Figure 3: Strouhal number-Reynolds number relationship for circular cylinder (Lienhard, 1966) (Achenbach & Heinecke, 1981) in (Blevins, 2001)

Natural Frequency

The natural frequency of the structure off which the vortices are shedding can be modeled using classic mechanics with slight variations for the particular construction of the device. Its equation is derived from:

$$f_n = \sqrt{\frac{k}{m}}$$

Equation 2: Natural frequency of a mass-spring system

Where

$$k = spring\ constant$$

$$m = effective\ mass$$

Which can be expressed through the equation

$$m = m_s + \frac{m_k}{3} + m_d$$

Where

$$m_s = mass\ of\ shredder\ beam$$

$$m_k = total\ mass\ of\ springs$$

$$m_d = mass\ of\ fluid\ displaced\ by\ the\ shedder\ system$$

Lift Force

The transverse lift force perpendicular to mean flow per unit length of cylinder is

$$F_L = \frac{1}{2}\rho U^2 D C_L \sin(\omega_s t)$$

Equation 3: Lift Force (Blevins, 2001)

Where:

$$\rho = fluid\ densiy\ in\ mass\ units, kg/m^3$$

$$U = free\ stream\ velocity, meters/sec$$

$$D = cylinder\ diameter, meters$$

$$C_L = lift\ coefficient, dimensionless$$

$$\omega_s = circular\ shedding\ frequency, \frac{rad}{sec} = 2\pi f_s$$

$$t = time, sec$$

Driven oscillator model

If the cylinder were constrained to a track, giving it one degree of freedom with equal range on either side and bounded by springs, its motion can be expressed through the equation

$$F_L = m\ddot{y} + 2m\zeta\omega_y\dot{y} + ky$$

Giving a direct relation of

$$m\ddot{y} + 2m\zeta\omega_n\dot{y} + ky = \frac{1}{2}\rho U^2 D C_L \sin(\omega_s t)$$

Equation 4: Driven Oscillator Model (Blevins, 2001)

Where

$$m = mass\ of\ shedder\ system$$

$$k = spring\ constant$$

$$\omega_n = circular\ natural\ frequency\ in\ \frac{rad}{sec} = 2\pi f_n$$

$$\zeta = damping\ factor$$

$$y = transverse\ displacement\ of\ shedder$$

$$\dot{y} = transverse\ velocity\ of\ shedder$$

$$\ddot{y} = transverse\ acceleration\ of\ shedder$$

Where the damping of a cylinder in viscous fluid at resonance is:

$$\zeta_{cly} = \frac{\pi}{2}\frac{\rho D^2}{m}\sqrt{\frac{v}{\pi f D^2}}$$

Equation 5: Damping of a Cylinder in Fluid Flow (Blevins, 2001)

Reduced Velocity

Reduced velocity is the ratio of the length of one cycle of vertices shed (Figure 2) and shedder diameter. It is present in steady vortex shedding conditions. It can be calculated using the following equation

$$U^* = \frac{U}{f_n D}$$

Equation 6: Reduced velocity

It is a non-dimensional parameter that can be used to quantify the relativity of flow velocity in terms of shedder system it is applied it.

Dimensionless Amplitude

Dimensionless amplitude is the ratio of amplitude and shedder diameter. It is present in steady vortex shedding conditions. It can be calculated using the following equation

$$A^* = \frac{A}{D}$$

Equation 7: Dimensionless amplitude

Where

$$A = Amplitude\ of\ voertex\ street$$

Where the whole width of the vortex path is *2A*. This non-dimensional parameter is useful in gauging the absolute amplitude of the shedder system, accounting for shedder diameter.

Past research

Volumes and volumes of research have been done on the phenomenon of VIV and more recently power generation harnessing energy generated by VIV. Focus will be directed on research which explores the effect of angle of incidence on VIV and more specifically, Strouhal number. Surrey & Surrey found a positive correlation in 1967 which can be seen in Figure 4.

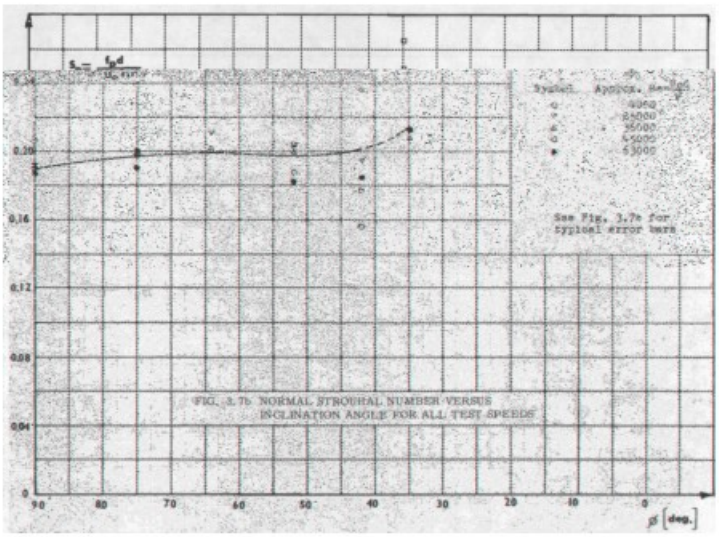

Figure 4: Normalized Strouhal number for fixed cylinder with different angles of inclination, 45 to 90 degrees. X-axis increases right to left. (Surry & Surry, 1967) in (Jain, 2012)

These graphs are from studies which were concerned with aeroelasticity. Their results may be more pronounced due to the relatively low effective mass of a structure in air as opposed to water and its lower damping coefficient due to air having a lower viscosity.

Franzini, et al.

Franzini, et al. conducted a practical experiment on vertically clamped cylinders of Plexiglas set at various angles of inclination in a fluid flow of $2000 < Re < 8000$ with up to 0.7 m/s flow velocity with low (<3%) turbulence. The angles at which the cylinders were tested were 0 (vertical), 20 and 45 degrees. This assembly was constrained to one degree of transverse motion and supported by springs and damped with air bearings. The cylinder assembly had a natural frequency of 0.48 Hz. The cylinder had a diameter of 32 mm and an immersed aspect ratio of 18 for every angle of inclination. The cylinder assembly had a mass damping ratio of 0.0125. There is a 3 mm parallel gap between the bottom of the cylinder and the floor of the test tank. A model of the test setup can be seen in Figure 6.

Their results found that angle of incidence has an effect on the reduced velocity at which lock-in occurs, as well as the amplitude of oscillations the shedder experiences. This is show in Figure 5.

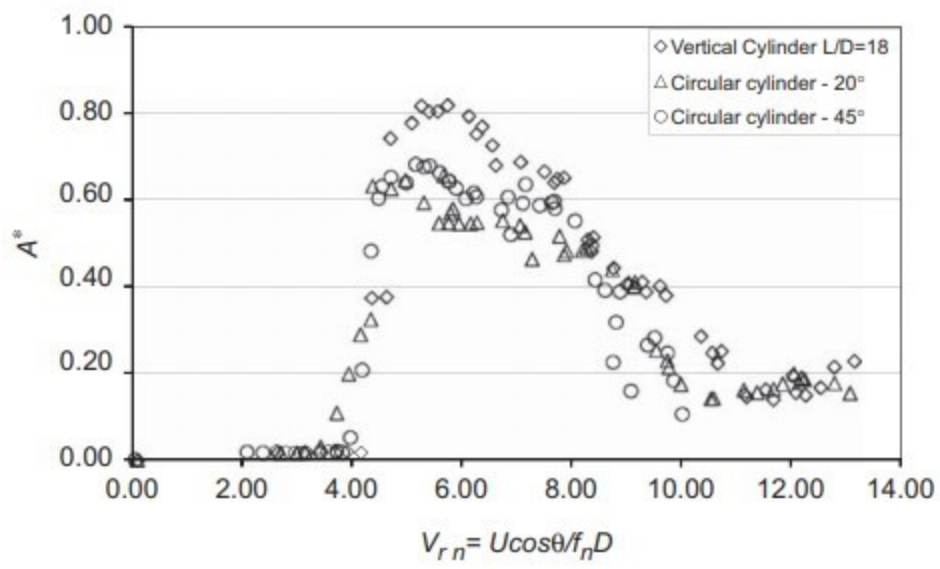

Figure 5: Effect of angle inclination on amplitude of a freely oscillating circular cylinder mounded on an elastic base (Franzini, Fujarra, Meneghini, Korkischko, & Franciss, 2009)

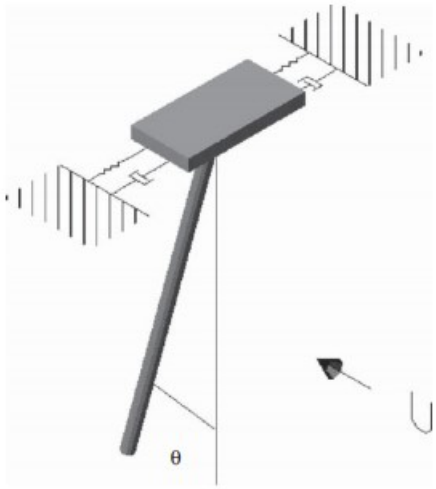

Figure 6: Convention of angular measurement used for the data in Figure 5 (Franzini, Fujarra, Meneghini, Korkischko, & Franciss, 2009)

Jain

Jain conducted a practical experiment in the same method as Franzini, et al. Flexibly mounted rigid cylinders of aluminum are set at various angles of inclination in a fluid flow of 500 < Re < 4000 with up to 0.3 m/s flow velocity with low (1%) turbulence. The angles at which the cylinders were tested were 0 (vertical), 20, 45, 55, 65 and 75 degrees. This assembly was constrained to one degree of transverse motion and supported by springs and damped with air bearings. The cylinder assembly had a natural frequency of 1 Hz. The cylinders had diameter of 12.7 mm and an immersed aspect ratio of 29 for every angle of inclination. The results used in this report were in the set where the cylinder assembly had mass damping factor of 0.029. There is a 1 mm parallel gap between the bottom of the cylinder and the floor of the test tank. A picture of the experimental setup can be seen in Figure 8.

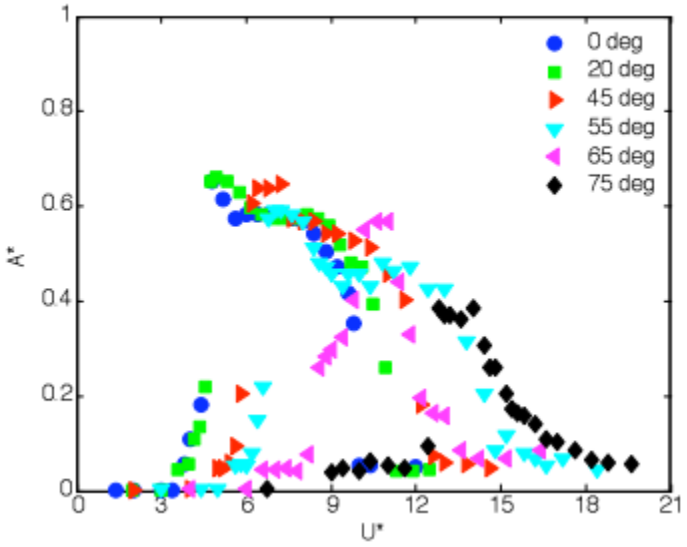

Figure 7: Amplitude vs reduced velocity for all angles of inclination, 1mm gap (Jain, 2012)

Angle of Inclination (θ)	Non-Dimensional Peak Amplitude (A*)
0°	0.64
20°	0.65
45°	0.64
55°	0.59
65°	0.57
75°	0.38

Table 1: Peak amplitudes for different angles of inclination (Jain, 2012)

Figure 8: Experimental setup (Jain, 2012)

Figure 9: Flow visualization in the wake of a) vertical cylinder, b) 45° inclined cylinder, c) 65° inclined cylinder, flow left-to-right (Jain, 2012)

Lunde & Østgård

Lunde & Østgård conducted a numerical analysis in three dimensions to find the effect of incline on flow around straight cylinders. Simulations were run for Re=150 and Re=1000. The angles at which the cylinders were tested were 0 (vertical), 15, 25, 35, 45, 55 and 65 degrees. A picture of the simulation can be seen in Figure 10.

Inclination angle α [°]	C_D	C'_L	C_p	S_t
0	1.3405	0.3685	-0.9245	0.1867
15	1.2506	0.3436	-0.8611	0.1800
25	1.1010	0.3019	-0.7581	0.1700
35	0.8995	0.2473	-0.6198	0.1533
45*	0.6657	0.0166	-0.4199	0.1798
55*	0.4404	0.0006	-0.2853	0.1698
65*	0.2401	0.0013	-0.1630	0.1521

*: Domain height 10D

Table 2: Flow quantities for different inclination angles, Re=150 (Lunde & Østgård, 2016)

Inclination angle α [°]	C_D	C'_L	C_p	S_t
0	1.0288	0.1225	-0.8870	0.2033-0.2100
15	0.9537	0.1126	-0.8175	0.2000-0.2033
25	0.8292	0.0781	-0.6995	0.1866-0.1900
35	0.6772	0.0594	-0.5668	0.1733
45*	0.4990	0.0374	-0.4126	0.1467-0.1533
55*	0.3320	0.0308	-0.2782	0.1133-0.1267
65*	0.1763	0.0049	-0.1448	0.1133-0.1666

*: Domain height 10D

Table 3: Flow quantities for different inclination angles, Re=1000 (Lunde & Østgård, 2016)

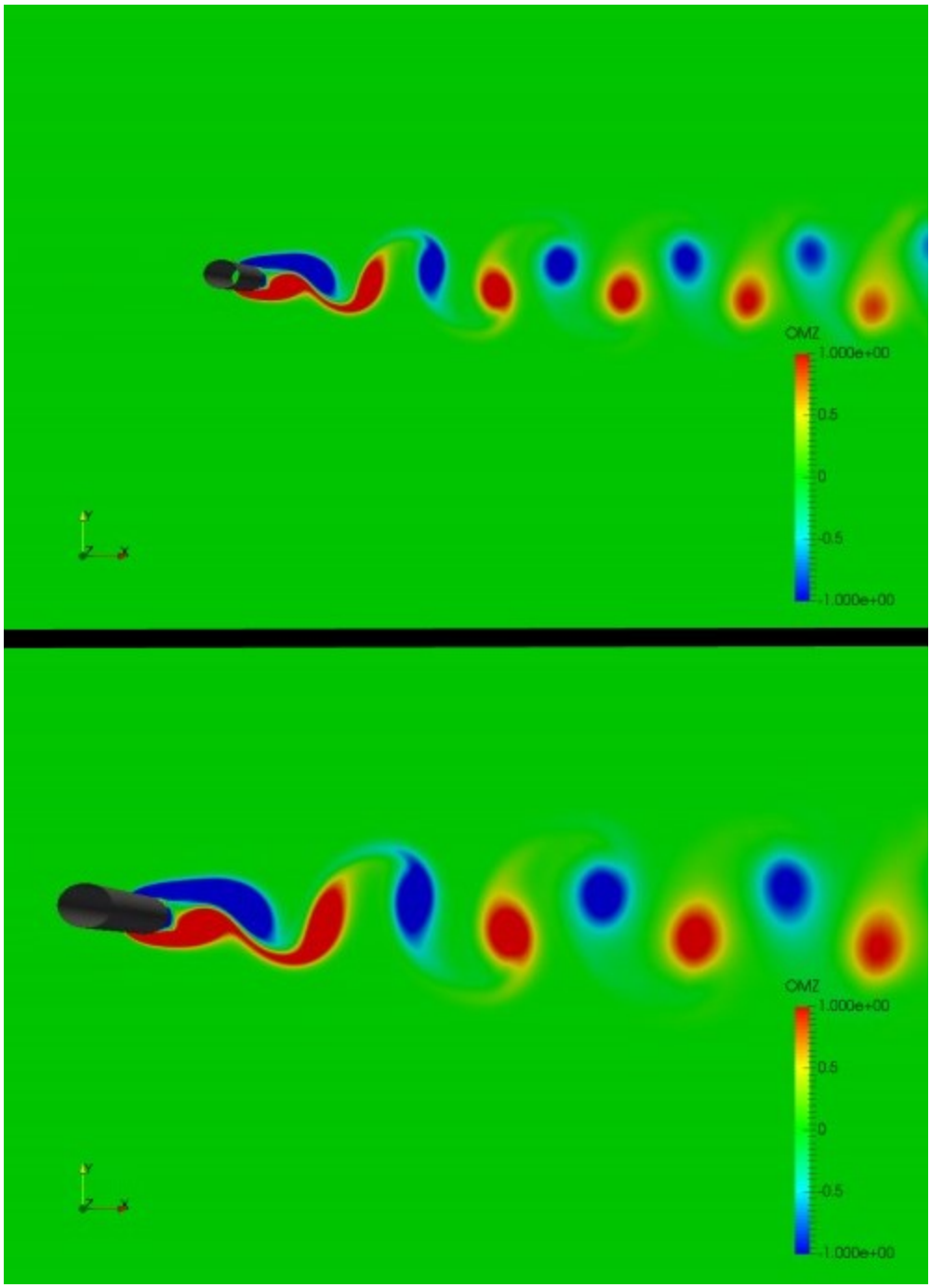

Figure 10: Experimental set up for simulation at 35 degrees (top) and 45 degrees (bottom) (Lunde & Østgård, 2016)

Analysis

Franzini

Figure 5 shows the effect that angle of inclination has on amplitude. This shows a reduction of amplitude caused by the angle of inclination, with an angle of 45 degrees reducing overall amplitude by approximately 0.18, or 22%. What this also shows is the shift of peak amplitude to lower values of reduced velocity as the angle of inclination is increased. The amplitude trend of a cylinder at a 45 degree angle reaches its apex at a reduced velocity of approximately 4.2 and begins its decline around 5 while the cylinder with 90 degree crossflow peaks at about 5.1 and does not start declining until about 6.5. This is a 57% reduction of the reduced velocity range in which lock-in occurs. It also demonstrates that a 45 degree angle of incidence shifts the reduced velocity at which lock-in begins by 0.9.

The benefits of a variable shedding frequency must be weighed against the costs of lost amplitude at increased angles of incidence.

This shows the effect that angle of inclination has on the velocity at which lock-in occurs, the range of velocities that lock-in is active on the cylinder and the overall amplitude at lock-in. These findings fit with the theory that an increased angle of inclination shifts the velocity at which lock-in occurs to a lower velocity.

Franzini's data shows that affecting the angle of incidence of a cylinder in fluid flow has an effect on overall amplitude and the reduced velocity at which lock-in begins. It would be possible to alter the angle of incidence to control the reduced velocity where lock-in is likely to occur. This would have a meaningful effect, based on this data.

The reduced velocity in which lock-in is observed lies in the range of $4 < U^* < 6$, except for the last measurement at 75 degrees.

Jain

In Figure 7, the reduced velocity at which lock-in begins can be seen to increase as angle of incidence is increased. At 0 and 20 degrees, lock-in begins at U*=4. At 45 degrees, lock-in begins at U*=5. At 55 degrees, lock-in begins at U*=6. At 65 degrees, lock-in begins at U*=8. At 75 degrees, lock-in begins at U*=12. Combining these results with Table 1, we are able to create an analytical table of Jain's results.

Angle of incidence (Θ)	Lock-in begins (U*)	Peak amplitude at lock-in (A*)
0	4	0.64
20	4	0.65
45	5	0.64
55	6	0.59
65	8	0.57
75	12	0.38

Table 4: Comparison of results (Jain, 2012)

Jain finds onset of lock-in region was delayed as angle of inclination was increased when plotted against reduced velocity. The reduced velocity in which lock-in is observed lies in the range of $4 < U^* < 6$, except for the last measurement at 75 degrees. These results supported and extend the findings in Franzini, et al., despite the difference in mass-damping factor. It can be concluded that mass-damping factor plays a relatively minor role in driving lock-in region and amplitude therein.

Lunde & Østgård

Lunde & Østgård conducted a numerical analysis in three dimensions to find the effect of incline on flow around straight cylinders. Their measurements were from a range of 0 to 65 degrees. Their results in the laminar and transition Reynolds number ranges (defined as $40 \leq Re \leq 150$ for laminar and $150 \leq Re \leq 300$ as transitional, see Figure 1) have supporting results. When the Reynolds number is increased to the subsritical range ($300 < Re < 1.5 \times 10^5$), an even stronger and more defined correlation occurs.

Table 5 displays results from Linde's experimental data shown in Table 2 with the Novak angle convention applied. These results are from experiments done at Re=250.

Table 6 displays results from Linde's experimental data shown in Table 3 with the Novak angle convention applied. These results are from experiments done at Re=1000.

Linde's experiments at Re=150 show results that are not in line with previous experiments, with Strouhal number decreasing along with the angle of inclination. When the Reynolds number of the experiment is increased to 1000, the results begin to appear similar to Chrust and Novak's experiments. The same trend of decreasing the angle of incidence results in an increased Strouhal number.

Linde saw a maximum change of 0.00367 Strouhal number per degree when the angle of incidence was changed from 45 to 35 degrees. Also, Lunde & Østgård saw a nearly 70% decrease in lift coefficient between a vertical cylinder and one at a 45 degree angle of incidence. This is 20% greater than the change noted in Franzini's experiments, although the results trend similarly.

Angle of incidence (Θ)	Strouhal number	Change in angle (degrees)	Change in Strouhal Number	$\frac{Change\ in\ Strouhal\ number}{Degree}$
0	0.1867			
15	0.18	15	0.0067	0.000447
25	0.17	10	0.01	0.001
35	0.1533	10	0.0167	0.00167
45	0.1798	10	-0.0265	-0.00265
55	0.1698	10	0.01	0.001
65	0.1521	10	0.0177	0.00177

Table 5: Extrapolated data from Table 2 to show angle's effect on Strouhal number in Linde's experiment, Re=150, Novak convention applied

Angle of incidence (Θ)	Strouhal number low	Strouhal number high	Strouhal number average	Change in angle (degrees)	Change in Strouhal Number	$\frac{Change\ in\ Strouhal\ number}{Degree}$
0	0.2033	0.21	0.20665			
15	0.2	0.2033	0.20165	15	0.00665	0.000443
25	0.1866	0.19	0.1883	10	0.01505	0.001505
35	0.1733	0.1733	0.1733	10	0.015	0.0015
45	0.1467	0.1533	0.15	10	0.0266	0.00266
55	0.1133	0.1267	0.12	10	0.0367	0.00367
65	0.1133	0.1666	0.13995	10	0.0067	0.00067

Table 6: Extrapolated data from Table 3 to show angle's effect on Strouhal number in Linde's experiment, Re=1000, Novak convention applied

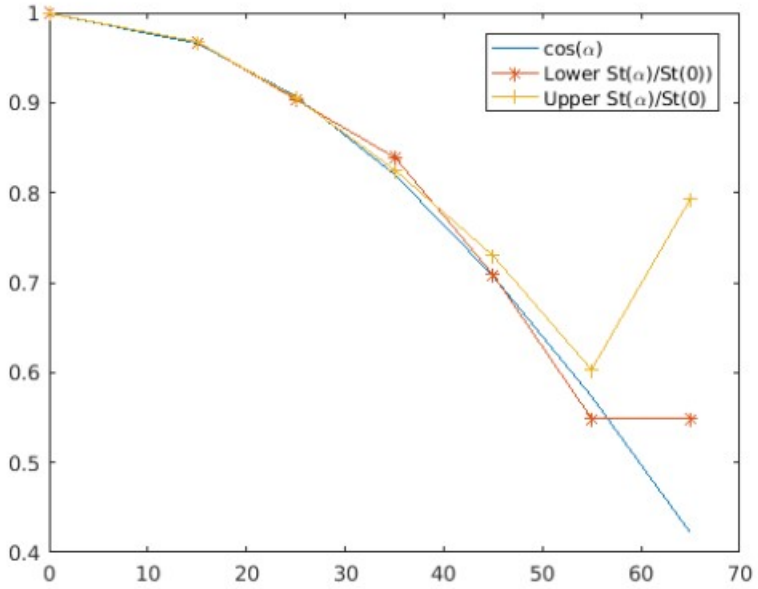

Figure 11: Normalized Strouhal number (x-axis) vs angle of inclination (y-axis), Re=1000 (Lunde & Østgård, 2016)

Angle of incidence (Θ)	Strouhal number (average)	Strouhal number normalized	Cos(Θ)	Error
0	0.207	1	1	0.000%
15	0.202	0.976	0.966	1.012%
25	0.188	0.911	0.906	0.537%
35	0.173	0.839	0.819	2.321%
45	0.150	0.726	0.707	2.584%
55	0.120	0.581	0.574	1.225%
65	0.140	0.677	0.423	37.596%

Table 7: Error between normalized Strouhal number and cosine transformation (Lunde & Østgård, 2016)

Discussion

If a shedder system were tuned properly to offer an angle of incidence to the direction of flow in response to flow velocity, the shedding frequency could be controlled to maintain singularity with natural frequency, shifting the onset of lock-in conditions. This would generate the maximum amplitude, force and acceleration possible for a range of flow velocities. It would also enable a single design to be placed in a variety of locations with only the need for simple tuning for specific conditions. It also minimizes the need to meter flow velocity, potentially avoiding solutions with a greater impact, such as damming.

Fixing the Strouhal number fixes the relationship between cylinder and fluid frequencies (Blevins, 2001). As flow velocity changes, so does the shedding frequency of the cylinder (Equation 1). To counter the resulting divergence of vortex shedding frequency and structure natural frequency, Strouhal number must be unfixed. Controlling Strouhal number will be key to maintaining lock-in conditions over a range of flow velocities.

The next step will be creating and applying a mathematical model to predict the influence angle of incidence has on Strouhal number, and apply that to methods to control the shedding frequency of the cylinder.

Methodology

This report proposes a method for counteracting the divergence from lock-in that would be introduced by transient flow velocity.

Lock-in occurs at or near the conditions which satisfy

$$f_s = f_n$$

Or

$$\frac{SU}{D} = \sqrt{\frac{k}{m}}$$

All physical parameters will be kept constant for this model, including cylinder diameter *D*, spring constant *k* and mass *m*. To maintain lock-in conditions, Strouhal number will have to be manipulated to counteract the changes in velocity.

Normalized Strouhal number is the ration between the Strouhal number experienced at a certain angle of incidence and the Strouhal number at 0 degrees. It can be represented by the equation

$$S_n = \frac{S_\theta}{S}$$

Equation 8: Normalized Strouhal number

Where

$$S = Strouhal\ number\ at\ 0\ degrees$$

$$S_\theta = Strouhal\ number\ at\ angle\ of\ incidence\ \theta$$

Table 7 shows that there exists a trigonometric relationship between angle of incidence and normalized Strouhal number at that angle. This can be represented by the equation

$$S_n \approx \cos(\theta)$$

Equation 9: Relationship between normalized Strouhal number and angle of inclination

This can be seen to be true within 3% margin of error for angles between 0 and 55 degrees (Lunde & Østgård, 2016).

Combining Equation 8 and Equation 9 and applying it toward Equation 1, we get a relationship for the shedding frequency at a particular angle of incidence, which can be expressed through the following equation

$$f_\theta = \cos(\theta)\frac{SU}{D}$$

Equation 10: Shedding frequency at angle of incidence

Since this relationship holds valid for angles from 0 to 55 (Table 7), those are the values that will be utilized. Applying the angles from Lunde & Østgård's experiment, we can use column 4 of Table 7 as a coefficient for modeling how angle will directly play into shedding frequency. This shows that increasing the angle of incidence lowers the value of its cosine, leading to the necessity of a greater flow velocity to achieve the same shedding frequency. This is exemplified in Table 8 below.

Θ	f_s	S	S_n	Cos(Θ)	U
Increase	Constant	Constant	Decrease	Decrease	Increase
Decrease	Constant	Constant	Increase	Increase	Decrease

Table 8: Relationships of variables with changing angle of incidence, to maintain resonance

If an apparatus were designed to dynamically change the angle of incidence in response to transient flow velocities, changes in flow velocity could cause the apparatus to "chase" the changing lock-in range and keep its shedding frequency in singularity with the natural frequency of the cylinder array. In order to do this, the apparatus would have to respond to increasing flow velocity by increasing the angle of incidence and vice versa.

Prototype Design

To keep the shedding frequency stagnant, the angle of incidence would need to be increased in a magnitude to directly counteract the increase in flow velocity. Lunde & Østgård's results in Table 7 show a dramatic change in Strouhal number along the range of 25-45 degrees while maintaining nearly maximum peak amplitude, as seen in Table 1.

The construction (Figure 8) and values for Jain's experiment will be used with one modification for the dynamic Strouhal number response. This will be a torsional spring of a known constant to variably control the angle of incidence in response to changing flow velocities (Figure 12).

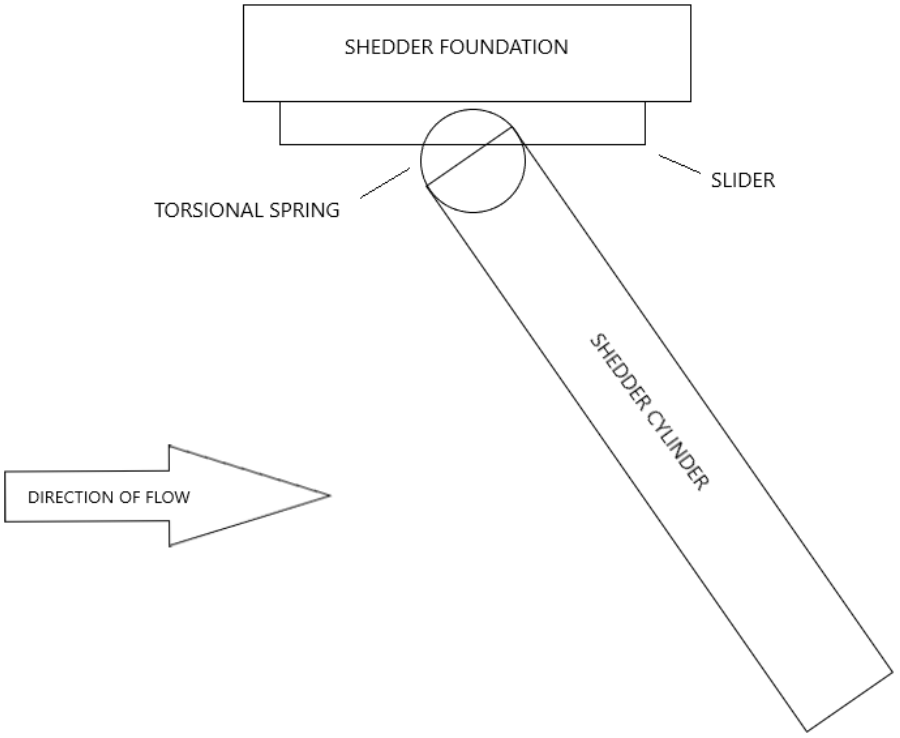

Figure 12: Schematic side view of modifications to Jain's setup to amplify placement of torsional spring

In Jain's experiment, the cylinder has a diameter of 12.7mm with immersed aspect ratio of 29, which translates to a cylinder length of 368.3 mm. The cylinder assembly has a natural frequency of 1 Hz. Lock-in is found to begin at a reduced velocity of 4. Using these variables in Equation 6, resonance (f_s = 1 Hz) is set to occur at a flow velocity of 0.0508 m/s. Inserting this result into Equation 1, it is now possible to solve for Strouhal number at 0 degrees. The result is 0.25; this is in the region of Strouhal numbers found in similar experiments and as such, it will be used.

To solve for the resultant flow velocity necessary to maintain lock-in at the baseline of 35 degrees angle of inclination, Equation 10 will be transformed to isolate flow velocity

$$U = \frac{D * f_n}{S * \cos(\theta)}$$

Equation 11: Flow velocity to maintain lock-in at known angle of inclination

Where if resonance is to be maintained, it will be true that

$$f_\theta = f_n$$

The values for flow velocity to maintain resonance at the angles in question are presented in Table 9. These flow velocities translate to reduced velocities (Equation 6), which are in line with Jain's findings seen in Figure 7 and Table 4. If an apparatus were set at a baseline of 35 degrees and tuned to tilt up or down 10 degrees, it would be possible to compensate for changes in flow velocity in a range of 0.0158 m/s while maintaining resonance.

With Strouhal number and cylinder diameter remaining constant and an apparatus compensating for changes in flow velocity by changing angle of incidence, flow velocity would be able to increase by 0.0098 m/s and decrease by 0.0060 m/s while still maintaining a perfectly matched resonance.

The force imparted by the flow of fluid at different velocities can be found using the equation

$$F = \frac{1}{2}\rho U^2 C_D R$$

Equation 12: Force imparted on shedder by fluid flow (Hall, 2015)

Where

$$\rho = density\ of\ fluid$$

$$C_D = drag\ coefficient$$

$$R = area\ normal\ to\ fluid\ flow$$

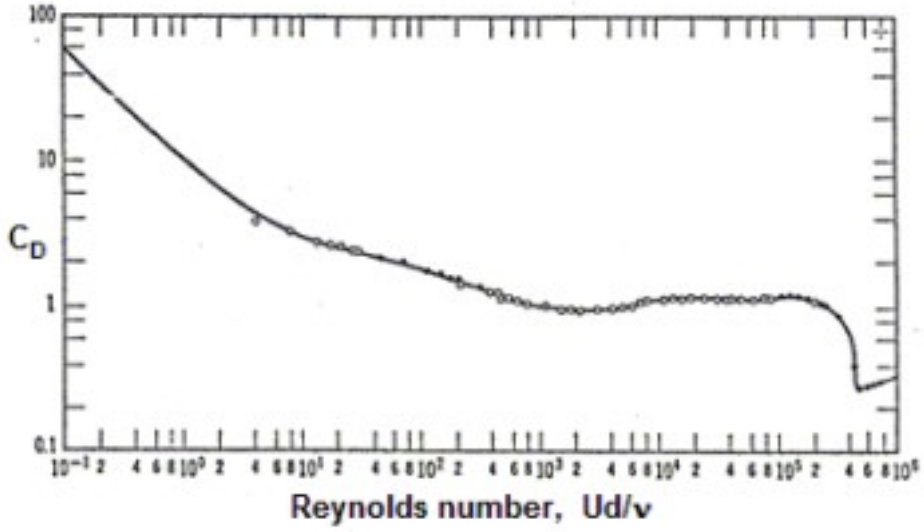

Figure 13: Drag coefficient for a circular cylinder as a function of Reynolds number (Brennen, 2006)

A value of 1000 will be used for Reynolds number. Using the graph in Figure 13, we get the value $C_D = 1$. The density for water will be a value of $\rho = 1000\ kg/m^3$. The surface area of the cylinder will be calculated with the equation

$$R = \pi r * l$$

Equation 13: Surface area of a cylinder

Where

$$r = radius\ of\ cylinder$$

$$l = length\ of\ cylinder$$

Here, the surface of the cylinder is $0.0147\ m^2$. Applying these values to Equation 12 for the different flow velocities gives the force values seen in Table 9.

The formula for finding the constant for a torsional spring is given by the equation

$$k_t = -\frac{\tau}{\theta}.$$

Equation 14: Spring constant of a torsional spring

Where

$$\tau = torque\ exerted\ by\ sprng\ (newton - meters)$$

$$\theta = angle\ of\ twist\ from\ equlibrium\ position\ (radians)$$

Assuming a homogeneous total force applied to the rigid cylinder by the fluid flow, we get the results in Table 9.

Angle of incidence (degrees)	Cos(Θ)	Flow velocity for resonance (m/s)	Reduced velocity at resonance	Force imparted by flow (N) (Equation 12)	Torque applied to shedder at spring (N*m)	Spring constant required (τ/radian)
0	1.0000	0.0508	4.0000	0.00947	0.00174	
25	0.9063	0.0561	4.4135	0.01153	0.00212	0.00487
35	0.8192	0.0620	4.8831	0.01412	0.00260	0.00426
45	0.7071	0.0718	5.6569	0.01895	0.00349	0.00444

Table 9: Values necessary to maintain resonance

A separate modeling is done to see the effects of scaling. The goal is to model a shedder that would operate in a faster current. The values for the experiment conducted by Ashok, et al. will be utilized and are included in Table 10. Values extrapolated in this experiment were Re=28539, S=0.1978 and f_s=7.787 Hz. These were applied to the method for determining the range of velocity which can be compensated for by altering the angle of incidence and the stiffness of the spring necessary to achieve this, if modeled as the prototype in Figure 12.

The flow velocity necessary to generate lock-in at normal cross-flow was calculated using Equation 11 and was found to be in line with Ashok, et al.'s maximum flow speed, 1 m/s. Applying Equation 11 for the same angles utilized in the previous model (25 degrees, 35 degrees, 45 degrees), we can see a theoretical allowance for an increase in flow velocity of 0.311 m/s while maintaining lock-in. If a dynamic shedder assembly with the design of the prototype in Figure 12 and the properties in Table 10 were tuned to respond dynamically to these conditions, it would need a radial spring with stiffness of approximately 1 N*m/radian. These results can be seen in Table 11.

Property	Parameter	Values
Cylinder material	M	PVC
Cylinder Diameter	D	25.4 mm
Cylinder Length	L	200 mm
Water density	$\rho fluid$	998 kg/m^3
Linear cylinder density	ρ_{cyl}	0.64 kg/m
Fluid temperature	T	25° C
Water Kinematic Density	v	0.89 e^{-6} m^2/s
Maximum Flow speed	U	1 m/s

Table 10: Known values for experiment conducted by Ashok, et al. (Ashok, Akshay, Akshatha, Akash, & Yogendra, 2019)

Angle of incidence (degrees)	Flow velocity at resonance (m/s)	Force of fluid on cylinder (N)	Torque exerted on spring (N*m)	Spring constant for resonance (N*m/radian)
0	0.9999	3.9794	0.3979	
25	1.1033	4.8447	0.4845	1.1103
35	1.2207	5.9305	0.5930	0.9708
45	1.4141	7.9588	0.7959	1.0133

Table 11: Results of modeling Ashok, et al.'s experiment of normal crossflow and applying an angle of incidence

Conclusions

It may be possible to drive the range of lock-in by actively controlling the angle of incidence of the shedder assembly. This would require fine tuning for exact conditions present, but once set, it could cover a range of velocities in a variable channel. This report found that starting at an angle of incidence of 25 degrees offset from vertical crossflow, the shedder cylinder could be set on a radial spring to passively respond to the change in flow velocity. Two models were put through the translation and it was found that angle of incidence could have an appreciable effect on the shedding frequency, possibly counteracting the divergence from natural frequency that occurs when flow velocity increases. These results are theoretical; it is recommended that a practical experiment be conducted to verify them.

Further Work

It is recommended that a practical experiment be set up to verify the methodology laid out in this report.

Works Cited

Achenbach, E., & Heinecke, E. (1981). On Vortex Shedding from Smooth and Rough Cylinders in the Range of Reynolds Numbers 6 x 103 to 5 x 106. *Journal of Fluid Mechanics*(109), 239-251. Retrieved 2020

Ashok, B. C., Akshay, B. L., Akshatha, H., Akash, D. L., & Yogendra, B. (2019, July). Design and Fabrication of Energy Harvester using VIVACE (Vortex Induced Vibrations Aquatic Clean Energy). *International Journal of Recent Technology and Engineering (IJRTE), 8*(2S3), 1023-1027. doi:10.35940/ijrte.B1192.0782S319

Bernitsas, M. M., Raghavan, K., Ben-Simon, Y., & Garcia, E. M. (2008). VIVACE (Vortex Induced Vibration Aquatic Clean Energy): A New Concept in Generation of Clean and Renewable Energy from Fluid Flow. *Journal of Offshore Mechanics and Arctic Engineering, 130*(4), pp. 041101-15.

Bishop, R. E., & Hassan, A. Y. (1964). The Lift and Drag Forces on a Circular Cylinder in a Flowing Fluid. *Proceedings of the Royal Society*, *Series A, 227*, pp. 51-75. London. Retrieved 2020

Blevins, R. D. (2001). *Flow-Induced Vibration* (Second ed.). Malabar, FL: Krieger Publishing Company. Retrieved 2020

Brennen, C. E. (2006). *Drag on a Sphere and Cylinder.* Retrieved 2020, from An Internet Book on Fluid Dynamics: http://brennen.caltech.edu/fluidbook/externalflows/drag/dragonasphere.pdf

Calvert, J. R. (1967). Experiments on the flow past an inclined disk. *Journal of Fluid Mechanics*(29), 691-703. Retrieved 2020

Chrust, M., Dauteuille, C., Bobinski, T., Rokicki, J., Goujon-Durand, S., Wesfreid, J. E., . . . Dusek, J. (2015). Ellect of inclination on the transition scenario in the wake of fixed disks and flat cylinders. *Journal of Fluid Mechanics*. doi:10.1017/jfm.2015.133

Franzini, G. R., Fujarra, A. L., Meneghini, J. R., Korkischko, I., & Franciss, R. (2009). Experimental investigation of Vortex-Induced Vibration on. *Journal of Fluids and Structures*(25), pp. 742-750. doi::10.1016/j.jfluidstructs.2009.01.003

Griffin, O. M., & Ramberg, S. E. (1974). The Vortex Street Wakes of Vibrating Cylinders. *Journal of Fluid Mechanics*(66), 553-576. Retrieved 2020

Hall, N. (Ed.). (2015). *The Drag Equation*. (G. R. Center, Producer) Retrieved 2020, from National Aeronautics and Space Administration: https://www.grc.nasa.gov/www/k-12/airplane/drageq.html

Hall-Stinson, A. S., Lehrman, C. J., & Tripp, E. R. (2011). *Energy Generation from Vortex Induced Vibrations.* Retrieved 2020, from WPI Digital Commons: https://digitalcommons.wpi.edu/mqp-all/79

Harish, A. (2020, January 27). *Why the Tacoma Narrows Bridge Collapsed: An Engineering Analysis*. Retrieved 2020, from SIMSCALE Blog: https://www.simscale.com/blog/2018/07/tacoma-narrows-bridge-collapse/

Jain, A. (2012). *Vortex-Induced Vibrations of an Inclined Cylinder.* Retrieved 2020, from UMass Amherst ScholarWorks: https://scholarworks.umass.edu/theses/911

Jing, X., Dongshi, W., Hui, H., Menglan, D., Jijun, G., & Chen, A. (2017). A vortex-induced vibration model for the fatigue analysis of a marine drilling riser. *Ships and Offshore Structures, 12*, 280-287. Retrieved 2020

Lienhard, J. H. (1966). *Synopsis of Lift, Drag and Vortex Frequency Data for Rigid Circular Cylinders.* Research Division Bulletin, Washington State University, College of Engineering.

Lunde, E., & Østgård, M. (2016). *Numerical investigation of flow around straight cylinders with inclination.* Norwegian University of Science and Technology, Marine Technology. Retrieved 2020

Mayforth, C., Doty, J. E., & Pratt, N. R. (2011). *Energy Generation from Vortex Induced Vibrations.* Retrieved 2020, from WPI Digital Commons: https://digitalcommons.wpi.edu/mqp-all/689

Novak, J. (1973). Strouhal Number and Flat Plate Oscillation in an Air Stream. *Acta Technica Csav*, pp. 372-386.

O'Connor, J. E., Wedell, J. R., Gagnon, J. A., & Diltz, N. L. (2017). *Vortex Induced Vibration Energy Harvesting through Piezoelectric Transducers.* Retrieved 2020, from WPI Digital Commons: https://digitalcommons.wpi.edu/mqp-all/846

Parkinson, G. V., & Brooks, N. P. (1961). On the Aerolastic Instability of Bluff Cylinders. *Journal of Applied Machanics*(28), 252-258. Retrieved 2020

Pierce, B. K., Neeld, C. J., Shipulski, E. E., & Ciliberto, F. R. (2019). *Small-Scale Vortex-Induced Vibration Wind Energy Harvesters.* Retrieved 2020, from WPI Digital Commons: https://digitalcommons.wpi.edu/mqp-all/6751

Surry, J., & Surry, D. (1967). *The effect of inclination on the Strouhal number and other wake properties of circular cylinders at subcritical Reynolds numbers.* Technical, University of Toronto, Institude for Aerospace Studies. Retrieved 2020

Warner, E. T., Ball, I. M., Sakhuja, S., & Killen, T. J. (2012). *Maximizing Vortex Induced Vibrations through Geometry Variation.* Retrieved from WPI Digital Commons: https://digitalcommons.wpi.edu/mqp-all/1213